

**A Model-Independent Determination of the Expansion and
Acceleration Rates of the Universe as a Function of Redshift and
Constraints on Dark Energy**

Ruth A. Daly

*Department of Physics, Berks-Lehigh Valley College, Pennsylvania State University,
Reading, PA, 19610*

and

S. G. Djorgovski

*Division of Physics, Mathematics, and Astronomy, California Institute of Technology,
MS 105-24, Pasadena, CA 91125*

ABSTRACT

Determination of the expansion and acceleration history of the universe is one of the fundamental goals of cosmology. Detailed measurements of these rates as a function of redshift can provide new physical insights into the nature and evolution of the dark energy, which apparently dominates the global dynamics of the universe at the present epoch. We present here dimensionless coordinate distances $y(z)$ to twenty radio galaxies reaching out to $z \approx 1.8$, the redshift range currently not covered by Supernova standard candle observations. We develop a simple numerical method for a direct determination of the expansion and acceleration rates, $E(z)$ and $q(z)$, from the data, which makes no assumptions about the underlying cosmological model or the equation of state parameter w . This differential method is in contrast the traditional cosmological tests, where particular model equations are integrated and then compared with the observations. The new approach is model-independent, but at a cost of being noisier and highly sensitive to the amount and quality of the available data. We illustrate the method by applying it to the currently available Supernova data and the data on radio galaxies presented here. We derive the expansion rate of the universe as a function of redshift, $E(z)$, and for the first time obtain a direct estimate of the acceleration rate of the universe as a function of redshift, $q(z)$, in a way that is independent of assumptions regarding the dark energy and its redshift evolution. The current observations indicate that the universe transitions from acceleration to deceleration at a redshift greater than 0.3, with a best fit estimate of about 0.45; this transition redshift and our determinations of $E(z)$ are broadly in agreement with the currently popular Friedmann-Lemaitre cosmology with $\Omega_m = 0.3$, and $\Omega_\Lambda = 0.7$, even though no model assumptions are made in deriving the fits for $E(z)$ and $q(z)$. With the advent of much better and richer data sets in the future, our direct method can provide a useful complementarity and an independent check to the traditional cosmological tests.

Subject headings: cosmological parameters - cosmology: observations - cosmology: theory - dark matter - equation of state

1. Introduction

A traditional task of cosmology is to determine the global geometry and dynamics of the universe. The field has been revolutionized by the modern measurements of CMBR fluctuations (e.g., Bennett et al. 2003, Spergel et al. 2003, and references therein), the use of distant supernovæ (SNe) in a Hubble diagram (see, e.g., Riess 2000, Leibundgut 2001, and references therein), radio galaxies (e.g. Daly & Guerra 2002), and many other advances. What these modern measurements have now convincingly demonstrated is that

the global mass/energy budget of the universe, and thus its dynamics, is dominated by a so-called dark energy component, which accounts for $\gtrsim 70\%$ of the closure density today. Einstein’s cosmological constant, Λ , is one special (and viable) case. More generally, this mysterious dark energy component is characterized through the equation of state, $w = p/\rho$, where p is the pressure and ρ the energy density; the cosmological constant solution corresponds to $w = -1$. For reviews and further references, see, e.g., Peebles & Ratra (2003), Padmanabhan (2003), or Turner (2002a, 2002b).

The nature of the dark energy (including its evolution in redshift, if any) is one of the most outstanding problems of physics and astronomy today. Constraining it through analysis of cosmological data is a task of a critical importance, and every new data set or analysis method can provide valuable insights into this problem.

Several recent studies have focused on the use of supernovae to determine the properties of the dark energy (Starobinsky 1998; Huterer & Turner 1999; Sani et al. 2000; Chiba & Nakamura 2000; Maor, Brustein, & Steinhardt 2001; Goliath et al. 2001; Astier 2001; Gerke & Efstathiou 2002; and Weller & Albrecht). The key ingredients are luminosity distances to sources over a broad range of redshift, preferably including sources at high redshift. Most of these analyses have focused on constraints on an evolving scalar field such as that used to define quintessence (Caldwell, Dave, & Steinhardt) or a rolling scalar field (Peebles & Ratra 1988). More recently, other types of models have been proposed to account for the acceleration of the universe, such as stringy dark energy (Frampton 2002) and k-essence (Armendariz-Picon, Damour, & Mukhanov 1999; Barger & Marfatia 2001).

Here, we focus on direct empirical determinations of the dimensionless expansion rate $E(z)$ and acceleration rate $q(z)$ and as functions of redshift. These require values for dimensionless coordinate distances to sources over a broad range of redshifts. We provide both a new data set, and a new method for estimating of $E(z)$ and $q(z)$.

We first present coordinate distances to 20 radio galaxies (RGs), reaching out to $z \approx 1.8$, and thus supplementing the existing SN data in what is a critical redshift regime. These RG data can be used to compare model predictions of any flavor of dark energy with the observations. These coordinate distances are derived and listed in §2. For completeness, and to compare the RG and supernova SN results, the coordinate distances to 78 SNe are also listed in §2. In §3, we derive the expressions for a direct determination of $E(z)$ and $q(z)$ from measurements of the dimensionless coordinate distances $y(z)$. In §4, we describe our simple numerical differentiation technique which can be used to implement these concepts on the real data. We illustrate the method and present our preliminary results based on the current RG and SN data sets in §5, and discuss implications for the properties of the dark energy in §6. A summary and discussion follows in §7.

2. Dimensionless Coordinate Distances

The values of coordinate distances to sources at high redshift can be used to determine or constrain global cosmological parameters, and to understand the properties and redshift evolution of the dark energy. Coordinate distances ($a_o r$) may be obtained from luminosity distances d_L or angular size distances d_A , since these are simply related to the coordinate distance: $d_L = (a_o r)(1 + z)$, and $d_A = (a_o r)/(1 + z)$.

The dimensionless coordinate distance, $y(z)$ is simply related to the coordinate distance $a_o r$, $y(z) = H_0(a_o r)$ (e.g., Peebles 1993). The luminosity distance d_L and the angular size distance d_A are also simply related to the dimensionless coordinate distance: $d_L = H_0^{-1} y(z) (1 + z) = H_0^{-1} D_L$, where D_L is the dimensionless luminosity distance (e.g. Perlmutter et al. 1999), and $d_A = H_0^{-1} y(z)/(1 + z)$.

Observations of supernovae type Ia and type IIb radio galaxies allow estimates of the dimensionless coordinate distances to sources at different redshift.

The use of FRIIb radio galaxies to determine the angular size distance or coordinate distance to radio galaxies at different redshifts is described in detail elsewhere (e.g. Podariu et al. 2003; Daly & Guerra 2002; Guerra, Daly, & Wan 2000). In addition to the use of FRIIb radio galaxies addressed here, other methods of using radio galaxies and quasars to determine coordinate distances are discussed by Buchalter et al. (1998), Gurvits, Kellermann, & Frey (1999), Vishwakarma (2001), Lima & Alcaniz (2002), and Chen & Ratra (2003). Here FRIIb radio galaxies are used to obtain dimensionless coordinate distances to 20 radio galaxies following the method described, for example, by Daly & Guerra (2002).

In the radio galaxy method proposed by Daly (1994), one model parameter β enters into the ratio $R_* \equiv < D > /D_*$; this ratio also depends on observed quantities and the dimensionless coordinate distance $y(z)$. In this model the ratio R_* is equal to a constant, κ :

$$R_*(\beta, y(z)) = \kappa. \quad (1)$$

The constants κ and β and their uncertainties are obtained by fitting all of the data to equation (1) (as described in detail by Guerra, Daly, & Wan 2000, and Daly & Guerra 2002, for example). The ratio is given by

$$R_* = k_o y^{(6\beta-1)/7} (k_1 y^{-4/7} + k_2)^{(\beta/3-1)}, \quad (2)$$

where k_o , k_1 , and k_2 are observed quantities (described in detail in the Appendix of Guerra, Daly, & Wan 2000). Equation (1) with R_* given by equation (2) allows a determination of $y(z)$ to each source; $y(z)$ is implicitly known for each source and is determined using an iterative technique. The values of y obtained along with the one σ error of y are listed in Table 1. In determining the one σ error bar on $y(z)$, the uncertainties of κ , k_o , k_1 ,

and β have been included; k_2 is known to high precision as it is the energy density of the microwave background radiation at the source redshift, and is the term that describes the effects of inverse Compton cooling of relativistic electrons by the microwave background radiation. The best fit values of κ and β vary slightly depending upon whether just the radio galaxy data are fit, or whether both the radio galaxy and supernova data are fit. Values of y obtained using the best fit parameters to radio galaxies alone are labeled y_s in Table 1, and those obtained using the best fit to both the radio galaxy and supernova data are labeled y_j . Note that the radio galaxy method does not rely upon a low-redshift normalization; the best fit value of κ is determined using all of the data.

The best fit values of κ , β , and \mathcal{M}_B (described below) and their error bars are included in Table 2, where the 54 supernovae included in the “primary fit C” of Perlmutter et al. (1999) and the 20 radio galaxies discussed here were studied. Values obtained from the fits of Daly & Guerra (2002) that allow for quintessence in a spatially flat universe with separate (s) and joint (j) fits to the radio galaxy and supernovae data are labelled “Q.” Best fit values obtained in the rolling scalar field model analyzed by Podariu et al. (2003) are labelled “SF.” As the number of data points in the fit increases, the value of each constant becomes independent of the assumptions of the fit. For example, the 54 supernovae points yield a consistent value of \mathcal{M}_B for fits that include supernovae only, or radio galaxies and supernovae, and in a universe with quintessence or a rolling scalar field. Since the value of \mathcal{M}_B changes so little when fit in different models, and when fit including or excluding radio galaxies, only one value of y is listed for each supernova. The 20 radio galaxy points show some small variations in the values of κ and β obtained with radio galaxies alone, or radio galaxies and supernovae, obtained in a universe with quintessence or a rolling scalar field. As more radio galaxy data points are added, the values of the constants will be more accurately determined. New runs were done that include the full 78 supernovae listed here and the best fit parameters and their error bars are the same as those listed in Table 2.

The coordinate distances to the supernovae are determined following the procedures of Perlmutter et al. (1999) and Riess et al. (1998). In the application of supernovae type Ia as a distance indicator, there is one model parameter α which is used to determine the effective apparent B band magnitude at maximum brightness m_B^{eff} . This is related to the dimensionless coordinate distance $y(z)$:

$$m_B^{eff}(\alpha) = \mathcal{M}_B + 5 \log[(1+z) y(z)] . \quad (3)$$

The constant \mathcal{M}_B is determined by fitting all of the supernova data, and is simply related to the absolute magnitude of the supernova peak brightness M_B : $\mathcal{M}_B = M_B + 25 - 5 \log H_0$ (see Perlmutter et al. 1999). Equation (3) is then used to determine $y(z)$ to each of the 54 supernovae in the “primary fit C” of Perlmutter et al. (1999), the 37 supernovae presented by Riess et al. (1998), and the 1 high-redshift supernova published by Riess et al. (2001), with the magnitude of this source corrected for gravitational lensing (Benitez et al. 2002).

The one σ uncertainty of y is obtained by combining the uncertainties of M_B and m_B^{eff} . These values are listed in Table 2. There are 14 sources that are present in both the Riess et al. (1998) and Perlmutter et al. (1999) samples used here. In the determinations of $E(z)$ and $q(z)$, average values of y with appropriate error bars were used for these duplicate sources; these values are listed in Table 4. The values of $y(z)$ are shown in Figures 1 and 2.

To test the reliability of the values of $y(z)$ obtained for the radio galaxies, a comparison was made between cosmological parameters obtained directly from the radio galaxy data alone and those obtained from the values of $y(z)$ listed in Table 1 in a quintessence model (see line 1 of Table 2). To do this, each value of y was substituted into equation (3) to obtain an equivalent effective apparent magnitude for the radio galaxy; the value of \mathcal{M}_B obtained for supernovae alone in a universe with quintessence (line 1 of Table 2) was adopted. These effective apparent magnitudes were then analyzed in a universe with quintessence, and the best fit parameters and their one sigma ranges compared with those obtained directly from the radio galaxy data. First, the χ^2 per degree of freedom went from 16.5/16 to 15.6/15, so the reduced χ^2 remains fairly constant; the number of degrees of freedom drops by one in the new fit since one new parameter, \mathcal{M}_B is fit. The one sigma range of Ω_m is 0.0 to 0.24 in the original fit, and is 0.0 to 0.17 in the new fit. The one sigma range of Ω_Q is 0.76 to 1.0 in the original fit, and is 0.83 to 1.0 in the new fit. The one sigma range of w in the original fit is -1.3 to -0.43 centered on -0.73, and is -1.5 to -0.56 centered on -0.8 in the new fit. The best fit value of \mathcal{M}_B is 23.83 ± 0.08 , compared with the value \mathcal{M}_B of 23.91 ± 0.03 used as an input to define an effective apparent magnitude for the radio galaxies. Thus, the cosmological parameters obtained directly from the radio galaxies are very similar to those obtained from the values of $y(z)$ listed in Table 1.

3. Computation of $E(z)$ and $q(z)$ from the Coordinate Distances

The determinations of the dimensionless coordinate distances do not require any assumptions regarding cosmological parameters, the dark energy, or the redshift evolution of these components once the values of the constants κ , β , and \mathcal{M}_B have been determined. In a universe with zero space curvature k as indicated by recent CMB measurements (e.g., Bennett et al. 2003, Spergel et al. 2003), it is straightforward to show using the Robertson-Walker line element and the relation $a(t)/a_o = (1+z)^{-1}$ that $H(z) \equiv \dot{a}/a = \sqrt{1-kr^2} (dy/dz)^{-1} H_0$, with $k=0$ and $H(z) = H_0 E(z)$,

$$E(z) = (dy/dz)^{-1} \quad (4)$$

(e.g. Peebles 1993; Weinberg 1972). Thus, in principle, the data $y(z)$ can be used to empirically determine the dimensionless expansion rate $E(z)$. This, in turn, is related to cosmological parameters, such as dark energy, and their redshift evolution as discussed in

§6.

For example, in a universe with quintessence (Caldwell, Dave, & Steinhardt 1998), which has a time-independent equation of state $w = P/\rho$, $E^2(z) = \sum \Omega_i(1+z)^{n_i}$, where $w_i = P_i/\rho_i$, and $n_i = 3(1+w_i)$ (see, for example, Turner & White 1997; Peebles & Ratra 2003; or Daly & Guerra 2002). The deceleration parameter at the present epoch is $q_o = -\ddot{a}a_o/\dot{a} = 0.5 \sum \Omega_i(1+3w_i)$, when w_i is time independent.

A direct, empirical determination of the acceleration of the universe as a function of redshift can be obtained from $y(z)$, without making any assumptions about the nature or evolution of the “dark energy.” This can be done using the equation (Daly 2002)

$$-q(z) \equiv \ddot{a}a/\dot{a}^2 = 1 + (1+z) (dy/dz)^{-1} (d^2y/dz^2) \quad (5)$$

valid for $k = 0$; if $k \neq 0$, another term $[kr(1+z)/(1-kr^2)](dr/dz)$ must be added to the right hand side of equation (5).

Equation (5) follows from the RW line element and the relation $(1+z) = a_o/a(t)$. Our measurements of the coordinate distance (a_{or}) move along the negative direction of dr , so eq. (2) with $k=0$ implies that $a_o dr = -(1+z) dt$, or $(dz/dt) = -a_o^{-1}(1+z) (dr/dz)^{-1}$. Differentiating $(1+z) = a_o/a(t)$ with respect to time implies that $\dot{a} = -a_o (1+z)^{-2} (dz/dt)$. Substituting in for (dz/dt) , we find $\dot{a} = (1+z)^{-1} (dr/dz)^{-1}$. Differentiating again with respect to time, we find $\ddot{a} = -(1+z)^{-2} (dz/dt) (dr/dz)^{-1} [1 + (1+z)(dr/dz)^{-1} (d^2r/dz^2)]$, which simplifies to eq. (5) using the expressions given here, and the relation $y(z) = H_0(a_{or})$.

Thus, equation (5) can in principle be used to empirically determine the redshift at which the universe transitions from acceleration to deceleration without requiring assumptions regarding the nature and redshift evolution of the “dark energy.” The supernova and radio galaxy data allow a determination of the dimensionless coordinate distance y to each source, at redshift z . These data can then be used to determine dy/dz , and d^2y/dz^2 ; these can then be substituted into eq. (5) to determine $q(z)$.

Since eqs. (4) and (5) are obtained without any assumptions regarding the mass-energy components of the universe or their redshift evolution, they can be used to directly determine the dimensionless acceleration rate $E(z) = (dy/dz)^{-1}$, which contains important information on the “dark energy” and its redshift evolution, and to determine the dimensionless acceleration parameter $q(z)$ directly from measurements of $y(z)$.

In the determinations of $y(z)$ a value of \mathcal{M}_B must be adopted for the supernovae (see eq. 3), and a value of κ must be adopted for radio galaxies (see eq. 1). There are not determined as a normalization using only low-redshift sources. They are determined by fitting all of the data and solving for the best fit values of these parameters. Fits to the supernovae data, the radio galaxy data, and the joint data set were run for a variety of cases (see Table 2), such as a universe with quintessence (Q), or a rolling scalar field (SF).

There are enough supernovae that the value of \mathcal{M}_B changes very little for different fits to the supernovae data, and they change very little if the supernovae data are considered separately or in conjunction with the radio galaxy data. Thus, values of y for supernovae do not change with the data set or model considered. The radio galaxy data best fit parameters for κ and β change slightly depending upon whether just the radio galaxies are considered, or whether the full data set of radio galaxies plus supernovae are included. Values of y_s obtained for the best fit value of κ using radio galaxies alone in a universe with quintessence are listed as well as the values y_j obtained using the best fit values of κ and β for fits to the full data set of radio galaxies and supernovae are listed in Table 1 and considered and compared in the analyses of $E(z)$ and $q(z)$.

4. The Numerical Differentiation Technique

The key problem in this approach, of course, is that it requires a numerical differentiation of typically noisy data, which is a cardinal sin for any empirical scientist. This, after all, is the reason why all standard cosmological tests (e.g., the Hubble diagram) consist of integrating the model equations to compare them with the measurements. An additional problem is posed by the sparse and/or uneven coverage of the redshift range(s) of interest. While a numerical differentiation of noisy data is in general not advisable, it is certainly possible, and if done properly (in a statistical sense), it can produce meaningful results within the limits of the available data.

Most numerical differentiation techniques explicitly or implicitly assume that the data can be locally represented by some smooth (differentiable) function, whose derivative is then defined analytically. Typically this local approximation is a low-order polynomial. Thus, estimation of derivatives is coupled with the estimation of the function representing the data themselves, in a self-consistent way. Measurement errors can then be propagated in the standard manner, leading to estimated uncertainties of the fitted function values as well as the derivatives. In our case, the function to be approximated, along with its first and second derivatives, is the dimensionless coordinate distance as a function of redshift, $y(z)$. The situation is simplified by the fact that the errors in z are negligible in comparison to the errors in y , and thus the ordinary least-squares approach can be used.

There are three sources of errors when evaluating any function fits to noisy, finite data sets. First, the errors of the individual data points: the least-squares approach deals with them in a statistically optimal fashion, provided that the quoted error bars are truly representative, and that the deviations from the “true” underlying trend are drawn from a normal distribution. Second, if the fitted function is not a good approximation to the true trend, the results may be systematically biased. Locally, any function can be approximated as a polynomial (or as a Taylor series), and this becomes an issue of a having a sufficiently high fit order to account for the shape (the curvature) of the observed trend in the fitting

interval. Finally, in any finite data set there will be some sample variance, i.e., a different draw of the same number of measurements from the same underlying trend, with the same errors, will produce slightly different results. The effects of the sample variance are minimised by having larger number of data points, and can be estimated numerically for any given sample.

We choose a simple powers-of- z polynomial approach, in order to be maximally model-independent. In principle, other basis functions could be used, but we do not see any advantages of such an approach in a situation where the fits would be dominated by the noise and sparse sampling of the data. We always fit to $y(z)$, and then derive the first and second derivatives from the fit coefficients, and the local values of $E(z)$ and $q(z)$ using eqs. (4) and (5). Uncertainties of the fit coefficients are then propagated to derive the uncertainties in the fit values of $y(z)$, $E(z)$ and $q(z)$. The fit values are always evaluated on a redshift grid equally and densely spaced in either z or $\log z$; this is just a matter of convenience, as the values and the quality of the fits are not affected.

A conceptually simplest approach would be to fit a polynomial to the entire data set. Unfortunately, low-order polynomials lack the flexibility to represent the actual shapes of underlying cosmological models, leading to seriously biased values of $E(z)$ and $q(z)$. The fits are (by design) optimised to fit the function (y), and its derivatives are not constrained directly. Using higher order polynomials helps in recovering the mean shapes of these functions, but at the expense of greatly increased uncertainties, and typically with some oscillatory behavior, characteristic of high-order polynomial fits. For example, the $q(z)$ is generally a non-linear function of z , so the fits of an order > 3 are needed; but in some cases, e.g., $\Omega_m = 1$ and $\Omega_\Lambda = 0$ cosmology, $q(z) = \text{const.}$, which higher order polynomials cannot reproduce very easily in shape, regardless of the increased errors for high-order terms.

A better method, which we adopted, is to fit the values of $y(z)$ locally, in some limited redshift window of $\pm\Delta z$; within that interval, data points are fitted with the weights inversely proportional to the squares of their error bars. In addition, at each end of the fitting window we attach a Gaussian tapered region with a $\sigma(z) = 0.02$, extending out to 2σ ; the enclosed data points in the tapered region have the weights lowered by the value of the Gaussian wing at that point. The purpose of this taper is to avoid fluctuations caused by individual data points entering and leaving the fitting window, at the expense of a slight increase in the resulting fit uncertainties (since the tapered points effectively get larger error bars). We established that the overall properties of the fits did not change. Finally, we require that there are at least 10 data points in each fit, and increment the window slightly if necessary.

The tradeoff is that larger fitting windows lead to more robust fits, at the expense of resolution in redshift and the introduction of the same problems which plague the global

polynomial fits, as described above; while smaller fitting windows produce noisier fits because of a smaller number of enclosed data points. After some experimentation, we concluded that windows with $\Delta z \approx 0.4$ seem to offer the optimal compromise, but we also perform fits with other window sizes.

After some experimentation, we decided to fit second order polynomials in each fitting window, as the minimal-assumption functions with defined second derivatives (needed to evaluate the $q(z)$), which can also accommodate any curvature in the data. We verified that using linear fits to obtain $y'(z)$ and thus $E(z)$ does not produce improved results, and that increasing the local fit order to 3 increases the formal errors without any significant benefits in terms of the fit quality and accuracy.

In exploring the numerical fitting and differentiation methodology, we used artificial data sets with known, built-in cosmologies, in order to evaluate the accuracy of the derived fits for $E(z)$ and $q(z)$. For most part, we generated artificial data sets mimicking what is expected from SN measurements by the SNAP satellite (see, e.g., Aldering et al. 2003, or <http://snap.lbl.gov/>), namely a set of 2000 measurements in the redshift interval from 0.1 to 1.7, with combined (measurement + intrinsic) scatter of 7% in dimensionless coordinate distances. The redshift distribution function was taken to be proportional to the volume element divided by the redshift, which roughly represents a combination of the expected SN rate history and the SNAP selection function. For most tests, we assumed the standard Friedmann-Lemaitre cosmology with $\Omega_m = 0.3$ and $\Omega_\Lambda = 0.7$. For some of the tests we changed some of these assumptions (the number of the data points, the relative errors, or the underlying cosmology).

The overall process is illustrated in Fig. 3, on an example of our pseudo-SNAP data set. The global trends for $y(z)$, $E(z)$, and $q(z)$ are reproduced well, with the bias (systematic offsets) comparable to the fit errors. The errors increase going towards the higher derivatives and near the edges of the redshift intervals, as may be expected.

The effects of different fitting windows on the derived values $y(z)$ and $E(z)$ are illustrated in Fig. 4. As expected, smaller values of Δz lead to noisier fits, but the overall trends agree within the errors. For the present RG+SN data set, we use Δz of 0.4 or 0.6 in what follows.

Finally, we address the issue of the sample variance. For our pseudo-SNAP data, we simply generate a number of different realizations of the data set, using the same assumptions. In order to estimate the effects for our RG+SN data set, we do the following. We assume an underlying cosmology, viz., $\Omega_m = 0.3$ and $\Omega_\Lambda = 0.7$. Then, we replace each $y(z)$ measurement with the value for this cosmology, perturbed by a random amount drawn from a Gaussian distribution with the $\sigma(y)$ equal to the quoted error bar. We generate a number of such pseudo-RGSN data sets, and perform the fits on each. The results are shown in Fig. 5. For the RG+SN data set, the sample variance effects are comparable to or

smaller than the measurement errors for $y(z)$; and comparable to the fitting uncertainties (which derive from the random errors of the data) for $E(z)$. As expected, the sample variance effects for the pseudo-SNAP data set, which has many more data points, are effectively negligible.

Estimates of the sample variance errors are made only rarely in the published literature. Our tests suggest that for many real-life data sets in cosmology, these errors can be easily comparable to the fitting uncertainties which derive from the random measurement errors, and thus in manu cases the quoted confidence intervals may be underestimating the total uncertainties.

5. The Initial Results for $E(z)$ and $q(z)$

Using the procedure described above, the function $E(z)$ was obtained for the full RG+SN data set, and is shown in Fig. 6. We used the values of y_j for RGs listed in Table 1, and the values for y for SNe listed in Tables 3 and 4; a total of 78 SNe were used including the average values of y for the 14 SNe listed in Table 4, and values of y for the remaining 64 SNe listed in Table 3. The results are remarkably close to the currently popular “concordance” Friedmann-Lemaître model with $\Omega_\Lambda = 0.7$ and $\Omega_m = 0.3$. We note, however, that in our analysis we did not assume that the universe is described by a Friedmann-Lemaître model at all.

As an internal consistency test, we computed the fits for the RG and SN samples separately, using the values y_s for the radio galaxies. The results are shown in Fig. 7. In the redshift range where the two samples overlap, these independent fits agree to within $1-\sigma$ (joint errors) or better. It is notable that the RG data alone are consistent with a constant $E(z) \approx 1.1$ for $z \sim 0.4 - 1.8$, although the error bars are large. If this trend remains as the error bars decrease with better and more extensive data sets, it could be indicative of an actual cosmological trend, or (perhaps more likely) some evolutionary effect or bias in the data. This can not be sorted out until more data are avialable.

Finally, we show in Fig. 8 what is probably the first direct estimate of $q(z)$. The data, folded through our analysis procedure, are fully consistent with the “concordance” model with $\Omega_\Lambda = 0.7$ and $\Omega_m = 0.3$, and suggest that indeed the universe transitions from deceleration to acceleration at $z_T \gtrsim 0.3$. Again, we note that no assumptions about the cosmological model have been made in deriving this trend. This is a preliminary result, and we are clearly limited by the available data at this time. Our purpose here is mainly to illustrate the method, but even so, the results are very encouraging.

6. Implications of $E(z)$ and $q(z)$ for the Properties of the Dark Energy

The acceleration parameter is $q(z) = -\ddot{a}/\dot{a}^2 = -(\ddot{a}/a)(\dot{a}/a)^{-2}$. The acceleration of the universe is described by

$$(\ddot{a}/a) = -\frac{4\pi G}{3} \sum (\rho_i + 3p_i) = -\frac{4\pi G}{3} \sum \rho_i(1 + 3w_i) \quad (6)$$

where p_i is the pressure, ρ_i is the mean mass-energy density, w_i is the equation of state of i th component, $w_i = p_i/\rho_i$. In addition, for $k = 0$,

$$(\dot{a}/a)^2 = \frac{8\pi G}{3} \sum \rho_i. \quad (7)$$

Thus, $q(z) = 0.5 \sum \rho_i(1 + 3w_i)/\sum \rho_i$ when $k = 0$, and $E^2(z) = \sum \rho_i/\rho_{co}$, where ρ_{co} is the critical density at the present epoch, $\rho_{co} \equiv (3/8\pi G)H_o^2 = \rho_{mo} + \rho_{Eo}$, and the present epoch mean mass-energy density of non-relativistic matter and dark energy are ρ_{mo} and ρ_{Eo} respectively. Non-relativistic matter evolves with redshift as $(1+z)^3$. Let the dark energy evolve with redshift as $f_E(z)$, then, it is easy to show that $E^2(z) = \Omega_m(1+z)^3 + (1-\Omega_m)f_E(z)$, where $\Omega_m = \rho_{mo}/\rho_{co}$, and $\Omega_E = \rho_{Eo}/\rho_{co} = 1 - \Omega_m$. Hence, if the current contribution of non-relativistic matter Ω_m can be determined, then $E(z)$ can be used to determine the redshift evolution of the dark energy $f_E(z)$. Similarly, $q(z) = 0.5[\Omega_m + (1-\Omega_m)(1+3w)(1+z)^{-3} f_E(z)]/[\Omega_m + (1-\Omega_m)(1+z)^{-3} f_E(z)]$.

Now, for quintessence, $\rho_i = \rho_{i,o}(1+z)_i^n$ when w_i is constant, where $n_i = 3(1+w_i)$. This follows from the mass-energy conservation of each component, which implies

$$\dot{\rho}_i = -3(\rho_i + p_i)(\dot{a}/a) \quad (8)$$

(e.g. Peebles 1993). When the equation of state w_i does not change with time, the solution to this equation is $\rho_i = \rho_{i,o}(1+z)^{3(1+w_i)}$, where $(1+z) = a_o/a$. Thus, a component with equation of state w_i and present mean mass-energy density ρ_o will have a mean mass-energy density at redshift z of $\rho = \rho_o(1+z)^{n_i}$, where $n_i = 3(1+w_i)$.

With two important components at low redshift, a non-relativistic component ρ_m that includes baryons and the dark matter in galaxies and clusters of galaxies, and a dark energy component ρ_E , we have $\rho_m = \rho_{mo}(1+z)^3$ and $\rho_E = \rho_{Eo}(1+z)^n$. Now, at zero redshift the total density is equal to the critical density $\rho_{co} = \rho_{mo} + \rho_{Eo}$ and since $\rho_{mo}/\rho_{oc} \equiv \Omega_m$, the acceleration parameter may be written

$$q(z) = 0.5 \left(\frac{\Omega_m + (1-\Omega_m)(1+3w)(1+z)^{3w}}{\Omega_m + (1-\Omega_m)(1+z)^{3w}} \right). \quad (9)$$

The universe is decelerating when the sign of $q(z)$ is positive. The sign of the denominator is always positive, and the numerator may be either positive or negative depending upon the value of w . The universe will go from a state of acceleration to a state of deceleration

if the dark energy has properties like that of quintessence when the numerator of equation (8) is positive, which occurs at the transition redshift z_T given by

$$z_T = \left[\frac{-\Omega_m}{(1+3w)(1-\Omega_m)} \right]^{1/(3w)} - 1. \quad (10)$$

This transition redshift is plotted as a function of the equation of state w in Figure 9. Clearly, as the transition redshift increases, the value of Ω_m must decrease, or the equation of state w exhibit redshift evolution.

Similarly, for quintessence, $E^2(z) = (1+z)^3[\Omega_m + (1-\Omega_m)(1+z)^{3w}]$. Some lines representing quintessence with $w = -1$ (i.e. a cosmological constant) are included in the figures.

Our preliminary results give a limit to the transition redshift $z_T \gtrsim 0.3$, with the best fit estimate $z_T \approx 0.45$. Assuming $\Omega_m = 0.3$, these translate to $w \lesssim -0.55$ and $-2.3 \lesssim w \lesssim -0.65$ (see Figure 9). With better data sets in the future, we should be able to improve on these limits.

7. Summary and Discussion

We presented here a set of dimensionless coordinate distances for 20 RGs, spanning the redshift range 0.43 to 1.79 (with one source at $z = 0.056$). These measurements supplement and extend to the cosmologically interesting redshift range the distances available for SNe, which currently reach only to $z = 0.97$ (with one source at $z = 1.70$).

The determination of the dimensionless coordinate distances to RGs and SNe are completely independent, and are based on completely different physics. Yet, the two data sets agree very well in the overlap redshift range, as shown here, and as shown by previous work (e.g., Podariu et al. 2002; Daly & Guerra 2002). This is very encouraging: there is a great value in being able to measure the same physical quantity (here the coordinate distances as a function of redshift) using different and independent tracers and methods. The general agreement we see between the SN and RG data sets suggests that neither method is dominated by some substantial, as yet unknown systematic errors. Together, the two data sets can be used in cosmological tests with a greater power than each data set separately.

The dimensionless coordinate distances $y(z)$ can be used to empirically determine the dimensionless expansion and deceleration rates as functions of redshift, $E(z)$ and $q(z)$, without assuming any particular cosmological model. While the traditional cosmological tests integrate the expressions for these functions provided by the models (e.g., the standard Friedmann-Lemaitre models) and determine the model parameters from the fits, we develop a complementary procedure whereby these functions can be derived directly

from the data by differentiating the $y(z)$ trend. We apply a particular, simple numerical procedure to this task, and derive the trends of both $E(z)$ and – for the first time – $q(z)$ directly from the data.

Our estimates of $E(z)$ are in an excellent agreement with those obtained from other methods, e.g., the CMBR fluctuations, high- z SNe, large-scale structure, etc., even though they are obtained in a completely different and independent manner. In particular, the data are consistent with the “concordance” cosmology, i.e., Friedmann-Lemaître models with $\Omega_m = 0.3$, and $\Omega_\Lambda = 0.7$. While these results are clearly very preliminary, and meant primarily to illustrate the method, the good agreement with other approaches is very encouraging.

We are currently limited by the amount and quality of the available data for both SNe and RGs. Nevertheless, there are great prospects for advances in precision cosmology, e.g., large sets of high-quality measurements of SNe from the SNAP satellite (e.g., Aldering et al. 2003), or from large ground-based experiments such as the ESSENCE (Stubbs 2002; see also <http://www.ctio.noao.edu/wproject/>) or LSST in the future (Tyson et al. 2002, 2003). Such data sets could certainly support differentiation of distance vs. redshift trends, leading to considerably more robust direct determinations of the expansion and acceleration rates as functions of redshift. In addition, new radio galaxy data is being obtained.

As the observational situation improves, direct estimates of $E(z)$ and $q(z)$ can be used to understand the properties and redshift evolution of different flavors of dark energy, determine the redshift at which the universe transitions from acceleration to deceleration, and may help elucidate any systematic errors that might be lurking in the RG or SN methods of constraining cosmological parameters.

It is a pleasure to thank Chris O’Dea, Megan Donahue, Eddie Guerra, Matt Mory, and Bharat Ratra for helpful discussions. This work was supported in part by the U. S. National Science Foundation under grants AST-0096077 and AST-0206002, and Penn State University (RAD), and by the Ajax Foundation (SGD).

REFERENCES

Aldering, G., et al. (the SNAP collaboration) 2003, Proc. SPIE, 4835, in press (astro-ph/0209550)

Armendariz-Picon, C., Damour, T., & Mukhanov, V. 1999, Phys. Lett. B, 458, 209

Astier, P. 2001, Phys. Lett. B, 500, 8

Barger, V., & Marfatia, D. 2001, Phys. Lett. B, 498, 67

Bennett, C., et al. (the WMAP team) 2003, *ApJ*, in press (astro-ph/0302207)

Caldwell, R. R., Dave, R., & Steinhardt, P. J. 1998, *Phys. Rev. Lett.*, 80, 1582

Chiba, T., & Nakamura, T. 2000, *Phys. Rev. D*, 62, 121301

Daly, R. A. 1994, *ApJ*, 426, 38

Daly, R. A. 2002, astro-ph/0212107

Daly, R. A., & Guerra, E. J. 2002, *AJ*, 124, 1831

Frampton, P. H. 2002, astro-ph/0209037

Gerke, B. F., & Efstathiou 2002, *MNRAS*, 335, 33

Goliath, M., Amanullah, T., Astier, P. Goobar, A., & Pain, R. 2001, *A&A*, 380, 6

Guerra, E. J., & Daly, R. A. 1998, *ApJ*, 493, 536

Guerra, E. J., Daly, R. A., & Wan, L. 2000, *ApJ*, 544, 659

Huterer, D., & Turner, M. S. 1999, *Phys. Rev. D*, 60, 081301

Leibundgut, B. 2001, *ARA&A*, 39, 67

Maor, I., Brustein, R., & Steinhardt, P. 2001, *Phys. Rev. Lett.*, 86, 6

Padmanabhan, T. 2003, *Phys. Rep.* in press (hep-th/0212290)

Peebles, P. J. E. 1993, *Principles of Physical Cosmology*, Princeton University Press

Peebles, P. J. E., & Ratra, B. 1998, *ApJ*, 325, L17

Peebles, P. J. E., & Ratra, B. 2003, *Rev. Mod. Phys.*, in press (astro-ph/0207347)

Perlmutter et al. 1999, *ApJ*, 517, 565

Podariu, S., Daly, R. A., Mory, M. P., & Ratra, B. 2003, *ApJ*, in press

Press, W., Teukolsky, S., Vetterling, W., & Flannery, B. 1992, *Numerical Recipes*, 2nd Edition. Cambridge: Cambridge Univ. Press

Riess, A. 2000, *PASP*, 112, 1284

Saini, T., Raychaudhury, S., Sahni, V., & Starobinsky, A. A. 2000, *Phys. Rev. Lett.*, 85, 1162

Spergel, D., et al. (the WMAP team) 2003, *ApJ*, in press (astro-ph/0302209)

Starobinsky, A., 1988, *JETP Lett.*, 68, 757

Stubbs, C. 2002, *BAAS*, 34, 1279

Turner, M. 2002a, *Int.J.Mod.Phys. A*17S1, 180-196 (astro-ph/0202008)

Turner, M. 2002b, in *Hubble's Science Legacy: Future Optical-Ultraviolet Astronomy from Space*, eds. K.R. Sembach et al., ASPCS, in press (astro-ph/0207297)

Turner, M.S. & White, M. 1997, *Phys. Rev. D*, 56, R4439

Tyson, J.A., et al. (the LSST collaboration) 2003, Proc. SPIE, 4836, 10 (astro-ph/0302102)

Tyson, J.A., Wittman, D., Hennawi, J., & Spergel, D. 2002, in Proc. 5th International UCLA Symposium on Sources and Detection of Dark Matter, ed. D. Cline, in press (astro-ph/0209632)

Weller, J., & Albrecht, A. 2002, Phys. Rev. D, 65, 103512

Weinberg, S. 1972, Gravitation and Cosmology, John Wiley & Sons

Table 1. Radio Galaxy Dimensionless Coordinate Distances

Source	Redshift	y_j	$\sigma(y_j)$	y_s	$\sigma(y_s)$
3C405	0.056	0.056	0.010	0.057	0.011
3C244.1	0.430	0.445	0.071	0.462	0.079
3C330	0.549	0.400	0.066	0.431	0.076
3C427.1	0.572	0.319	0.051	0.319	0.054
3C337	0.630	0.600	0.071	0.630	0.080
3C55	0.720	0.606	0.071	0.680	0.085
3C247	0.749	0.625	0.069	0.660	0.077
3C265	0.811	0.667	0.081	0.731	0.093
3C325	0.860	0.818	0.149	0.885	0.162
3C289	0.967	0.681	0.108	0.722	0.122
3C268.1	0.974	0.780	0.127	0.855	0.149
3C280	0.996	0.703	0.111	0.758	0.128
3C356	1.079	0.842	0.151	0.979	0.188
3C267	1.144	0.753	0.126	0.837	0.150
3C194	1.190	1.141	0.205	1.251	0.239
3C324	1.210	0.996	0.251	1.081	0.291
3C437	1.480	0.849	0.206	0.992	0.260
3C68.2	1.575	1.477	0.386	1.717	0.484
3C322	1.681	1.167	0.249	1.356	0.316
3C239	1.790	1.246	0.257	1.419	0.318

Table 2. Best Fit Parameters

Model	Fit To	\mathcal{M}_B	κ	β	$\frac{\chi^2}{dof}$ (SN)	$\frac{\chi^2}{dof}$ (RG)
Q	SN/RG only (s)	23.91 ± 0.03	8.88 ± 0.05	1.70 ± 0.04	56.2/50	16.53/16
Q	SN+RG (j)	23.95 ± 0.03	8.81 ± 0.05	1.75 ± 0.04	74.1/68	74.1/68
SF	SN/RG only (s)	23.94 ± 0.03	8.90 ± 0.05	1.70 ± 0.04	56.7/50	16.7/16
SF	SN+RG (j)	23.95 ± 0.03	8.81 ± 0.05	1.80 ± 0.03	74.1/68	74.1/68

Table 3. Supernovae Ia Dimensionless Coordinate Distances

Source	Redshift	y_s	$\sigma(y_s)$	ref
1996C	0.009	0.008	0.0012	R98
1995D	0.012	0.011	0.0011	R98
1992al	0.014	0.013	0.0013	P99
1992al	0.014	0.013	0.0009	R98
1995ak	0.016	0.015	0.0014	R98
1994S	0.016	0.015	0.0010	R98
1992bo	0.018	0.019	0.0016	R98
1992bc	0.020	0.017	0.0016	P99
1992bc	0.020	0.020	0.0012	R98
1995ac	0.022	0.023	0.0018	R98
1994M	0.024	0.026	0.0022	R98
1993H	0.025	0.024	0.0029	R98
1992ag	0.026	0.026	0.0028	R98
1992ag	0.026	0.029	0.0027	P99
1992P	0.026	0.026	0.0029	P99
1992P	0.026	0.030	0.0020	R98
1995bd	0.028	0.034	0.0033	R98
1999O	0.030	0.028	0.0026	P99
1992bg	0.035	0.038	0.0038	R98
1994T	0.036	0.035	0.0035	R98
1992bg	0.036	0.034	0.0033	P99
1992bl	0.043	0.043	0.0036	P99
1992bl	0.043	0.038	0.0026	R98
1992bh	0.045	0.051	0.0040	R98
1992bh	0.045	0.052	0.0046	P99
1995E	0.049	0.049	0.0031	R98
1990af	0.050	0.052	0.0044	P99
1993ag	0.050	0.054	0.0050	P99
1993ag	0.050	0.048	0.0038	R98
1990af	0.050	0.042	0.0031	R98
1993O	0.052	0.053	0.0030	R98
1993O	0.052	0.050	0.0042	P99

Table 3—Continued

Source	Redshift	y_s	$\sigma(y_s)$	ref
1992bs	0.063	0.068	0.0057	P99
1992bs	0.064	0.069	0.0045	R98
1993B	0.071	0.071	0.0065	P99
1992ae	0.075	0.074	0.0058	R98
1992ae	0.075	0.074	0.0068	P99
1992bp	0.079	0.068	0.0057	P99
1992bp	0.080	0.069	0.0044	R98
1992br	0.087	0.087	0.0077	R98
1992aq	0.101	0.096	0.0067	R98
1992aq	0.101	0.101	0.0107	P99
1996ab	0.124	0.124	0.0073	R98
1997I	0.172	0.151	0.0126	P99
1997N	0.180	0.169	0.0133	P99
1996J	0.300	0.319	0.0357	R98
1997ac	0.320	0.291	0.0243	P99
1994F	0.354	0.361	0.0549	P99
1994am	0.372	0.337	0.0312	P99
1994an	0.378	0.389	0.0663	P99
1996K	0.380	0.337	0.0310	R98
1995ba	0.388	0.399	0.0369	P99
1995aw	0.400	0.346	0.0304	P99
1997am	0.416	0.376	0.0349	P99
1994al	0.420	0.372	0.0430	P99
1994G	0.425	0.305	0.0690	P99
1996E	0.425	0.344	0.0449	R98
1997Q	0.430	0.373	0.0311	P99
1996U	0.430	0.497	0.0574	R98
1997ce	0.440	0.375	0.0304	R98
1995az	0.450	0.358	0.0380	P99
1996cm	0.450	0.485	0.0515	P99
1997ai	0.450	0.414	0.0574	P99
1995aq	0.453	0.484	0.0559	P99

Table 3—Continued

Source	Redshift	y_s	$\sigma(y_s)$	ref
1992bi	0.458	0.469	0.0994	P99
1995ar	0.465	0.516	0.0715	P99
1997P	0.472	0.464	0.0409	P99
1995K	0.478	0.459	0.0353	R98
1995ay	0.480	0.431	0.0478	P99
1996ci	0.495	0.402	0.0354	P99
1995as	0.498	0.602	0.0695	P99
1997cj	0.500	0.442	0.0340	R98
1997H	0.526	0.456	0.0423	P99
1997L	0.550	0.530	0.0613	P99
1996cf	0.570	0.469	0.0477	P99
1996I	0.570	0.499	0.0430	R98
1997af	0.579	0.513	0.0522	P99
1997F	0.580	0.508	0.0541	P99
1997aj	0.581	0.428	0.0436	P99
1997K	0.592	0.785	0.1340	P99
1997S	0.612	0.554	0.0538	P99
1995ax	0.615	0.439	0.0507	P99
1997J	0.619	0.580	0.0750	P99
1996H	0.621	0.535	0.0434	R98
1995at	0.655	0.445	0.0432	P99
1996ck	0.656	0.510	0.0660	P99
1997R	0.657	0.575	0.0611	P99
1997G	0.763	0.725	0.1772	P99
1996cl	0.828	0.760	0.1892	P99
1997ap	0.830	0.652	0.0664	P99
1997ck	0.970	0.844	0.1169	R98
1997ff	1.700	0.967	0.1517	R02

Table 4. Average Values of y for Supernovae Listed by Both R98 and P99

Source	Redshift	y_s	$\sigma(y_s)$
1990af	0.050	0.047	0.0053
1992ae	0.075	0.074	0.0090
1992ag	0.026	0.027	0.0039
1992al	0.014	0.013	0.0016
1992aq	0.101	0.098	0.0126
1992bc	0.020	0.019	0.0020
1992bg	0.036	0.036	0.0050
1992bh	0.045	0.051	0.0061
1992bl	0.043	0.040	0.0044
1992bp	0.079	0.069	0.0072
1992bs	0.063	0.069	0.0073
1992P	0.026	0.028	0.0035
1993ag	0.050	0.051	0.0063
1993O	0.052	0.052	0.0051

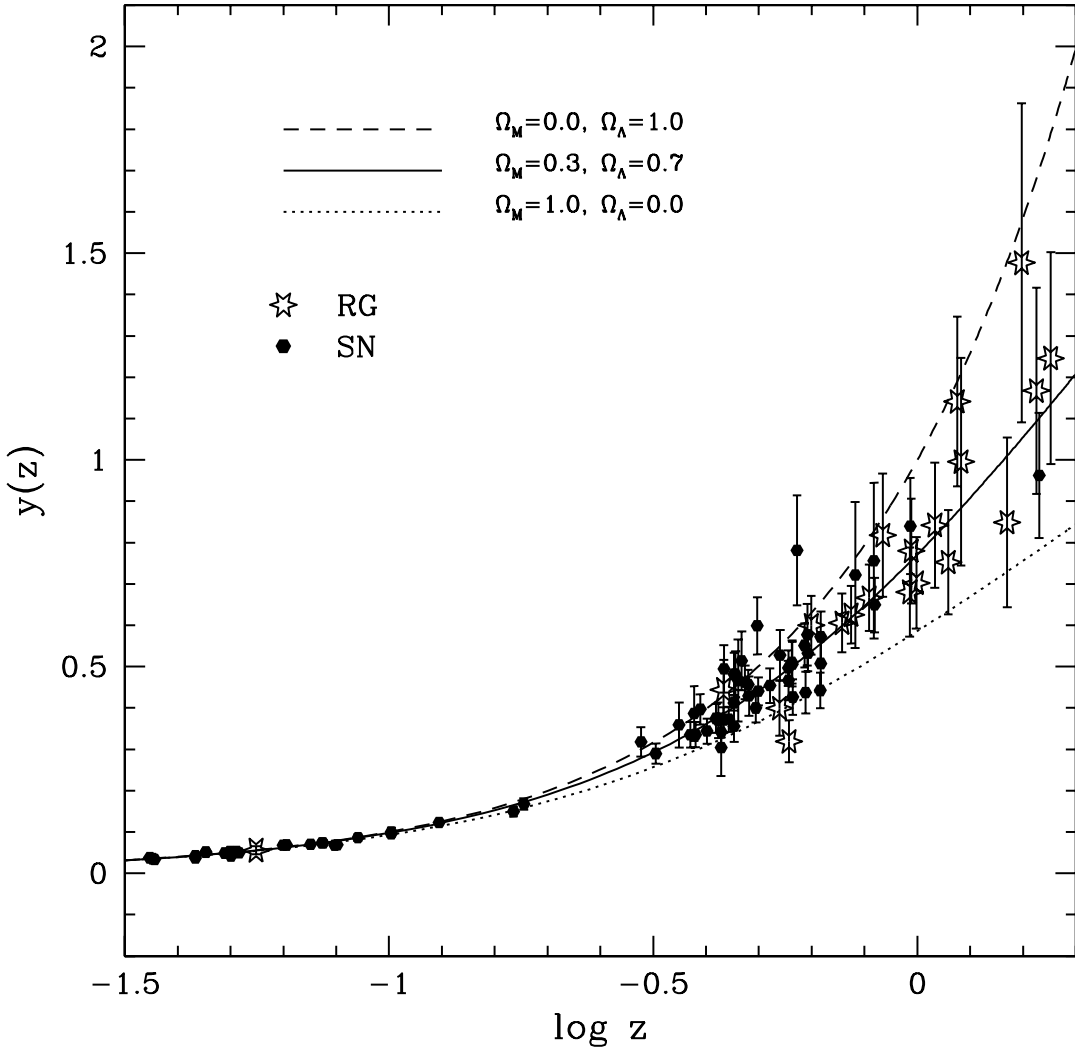


Fig. 1.— Dimensionless coordinate distances $y(z)$ to 20 radio galaxies and 78 supernovae as a function of $\log z$. Note that the determinations of $y(z)$ have been made using best fit value of \mathcal{M}_B obtained for the full data set of 78 supernovae and 20 radio galaxies, and the best fit value of κ obtained using the full data set (y_j for radio galaxies). Radio galaxies are shown as open stars and supernovae are shown as solid circles. Very similar results obtain when values of y_s for radio galaxies are shown.

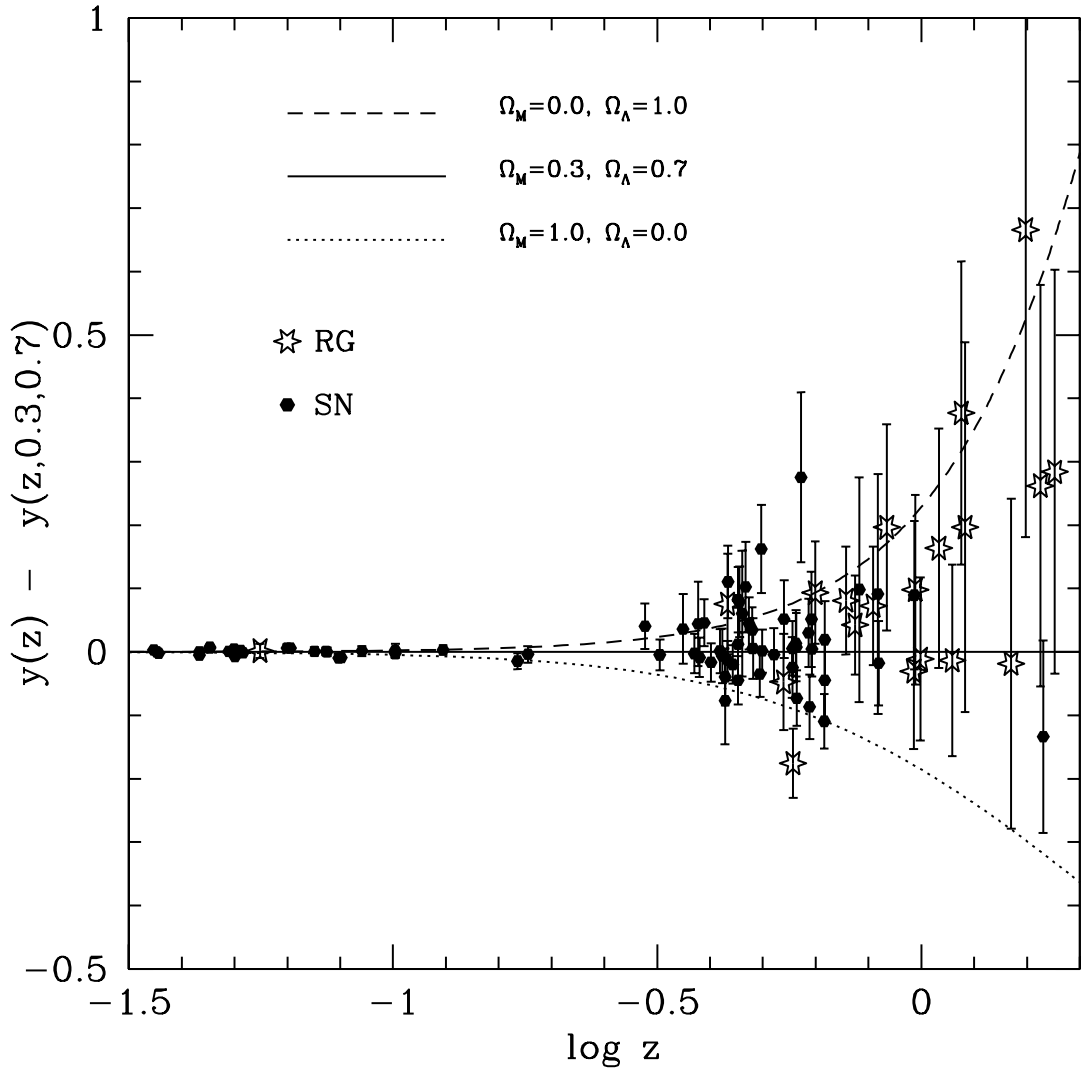


Fig. 2.— The residuals between $y(z)$ and those expected in a universe with $\Omega_m = 0.3$ and $\Omega_\Lambda = 0.7$, where $y(z)$ is the dimensionless coordinate distance, shown as a function of $\log z$. Values of y_s , obtained using the best fit value of κ obtained for radio galaxies alone, are shown. The results obtained when best fit values to the full data set are used are very similar. Radio galaxies are shown as open stars and supernovae are shown as solid circles.

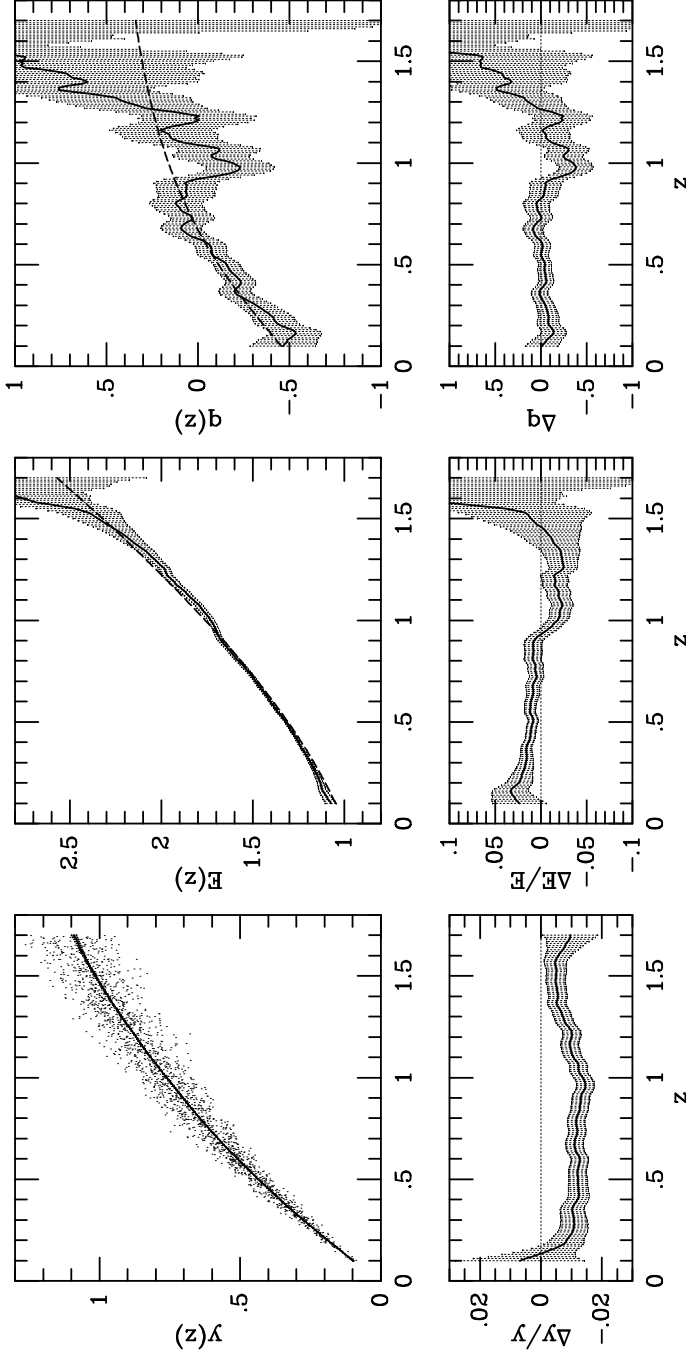


Fig. 3.— An example of the sliding-window fitting results for a pseudo-SNAP data set with 2000 data points. We assumed the cosmology with $\Omega_m = 0.3$ and $\Omega_\Lambda = 0.7$, and the relative errors $\Delta y/y$ drawn from a Gaussian distribution with $\sigma = 7\%$. The top left panel shows the input data (dots) along with the recovered $y(z)$ trend. The bottom left panel shows the $y(z)$ fit residuals from the values corresponding to the assumed cosmology. The middle panels show the fits for $E(z)$ (top) and its residuals (bottom), and the right panels the equivalent for $q(z)$. In all cases the thick line shows the fit values, and the hashed area indicates the $\pm 1\sigma$ uncertainties. In the top middle and right panels, the dashed lines show the theoretical values for the assumed cosmology.

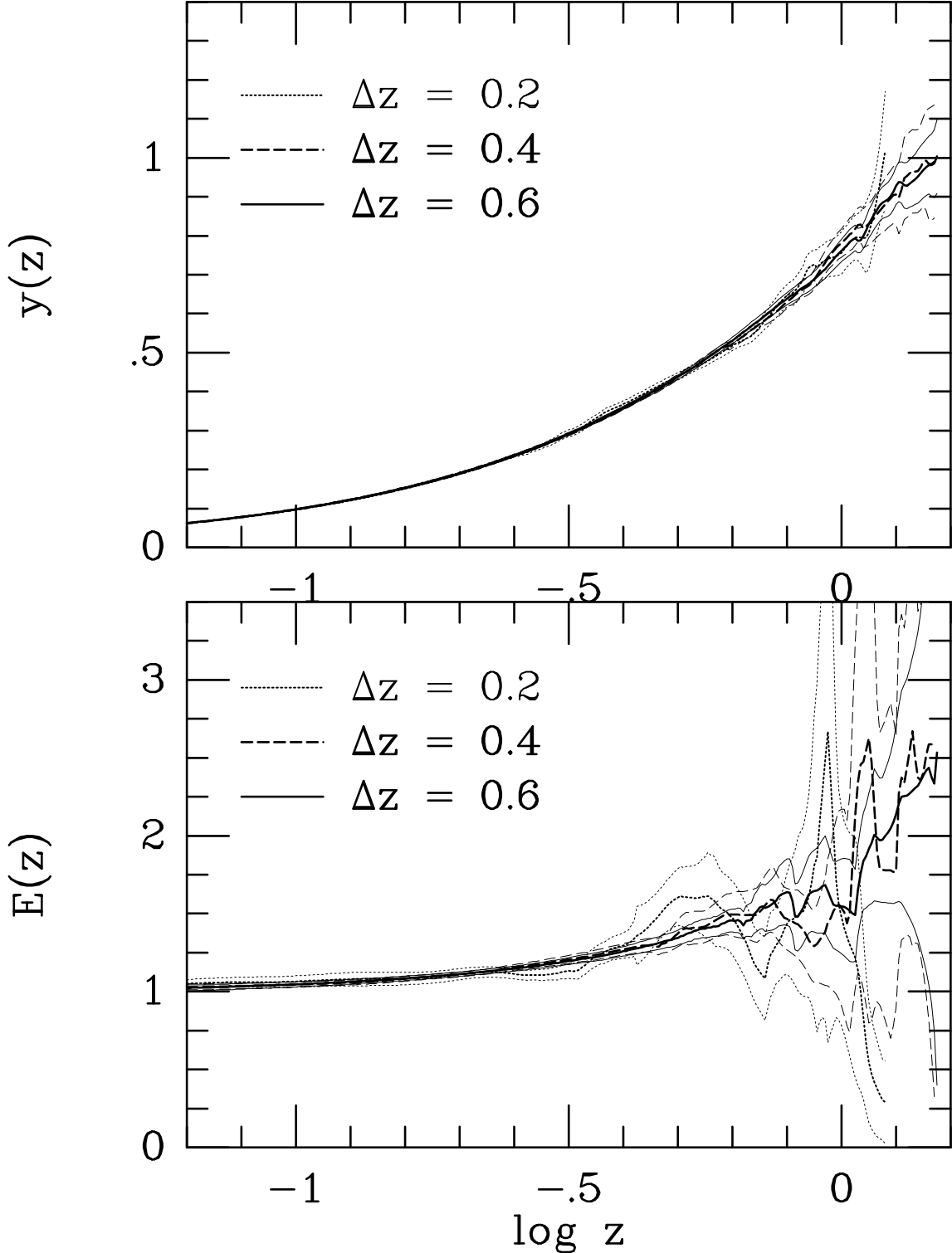


Fig. 4.— Comparison of results obtained for $E(z)$ when different fitting window functions are applied to the full data set of 20 radio galaxies and 78 supernovae; values of y_j for the radio galaxies were used for these fits. Examples of three different window functions are shown with different line types, as indicated. The fit values are indicated by the thick lines, whereas the corresponding thin lines indicate the $\pm 1\sigma$ range.

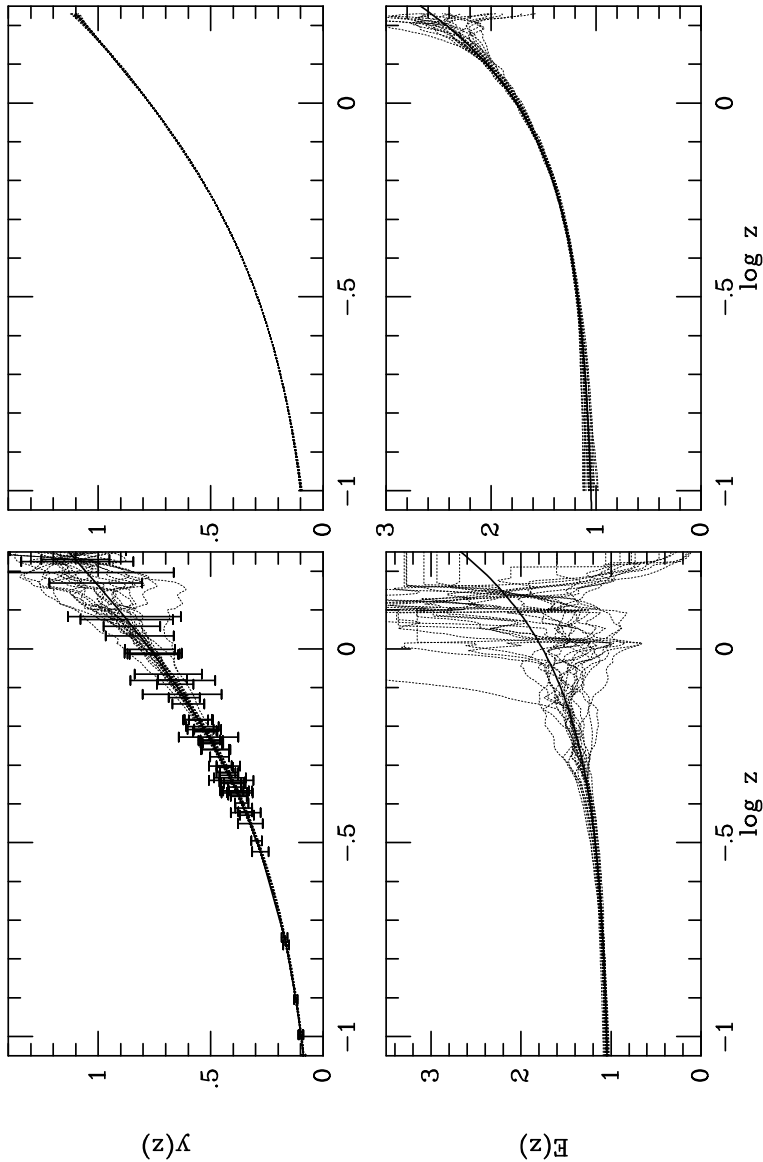


Fig. 5.— Modeling of the sample variance effects for the RG+SN sample (left) and the pseudo-SNAP sample (right). A cosmology with $\Omega_m = 0.3$, and $\Omega_\Lambda = 0.7$ was assumed, and is shown with the solid lines in each panel. The placement and the error bars of the SN+RG data points are also indicated in the top left panel. Each dotted line represents a fit from a single random realization of the mock data sets, as described in the text. Their spread at a given redshift is indicative of the sample variance errors. These are obviously much more significant for the smaller- N , RG+SN data set, than for the much larger pseudo-SNAP data set.

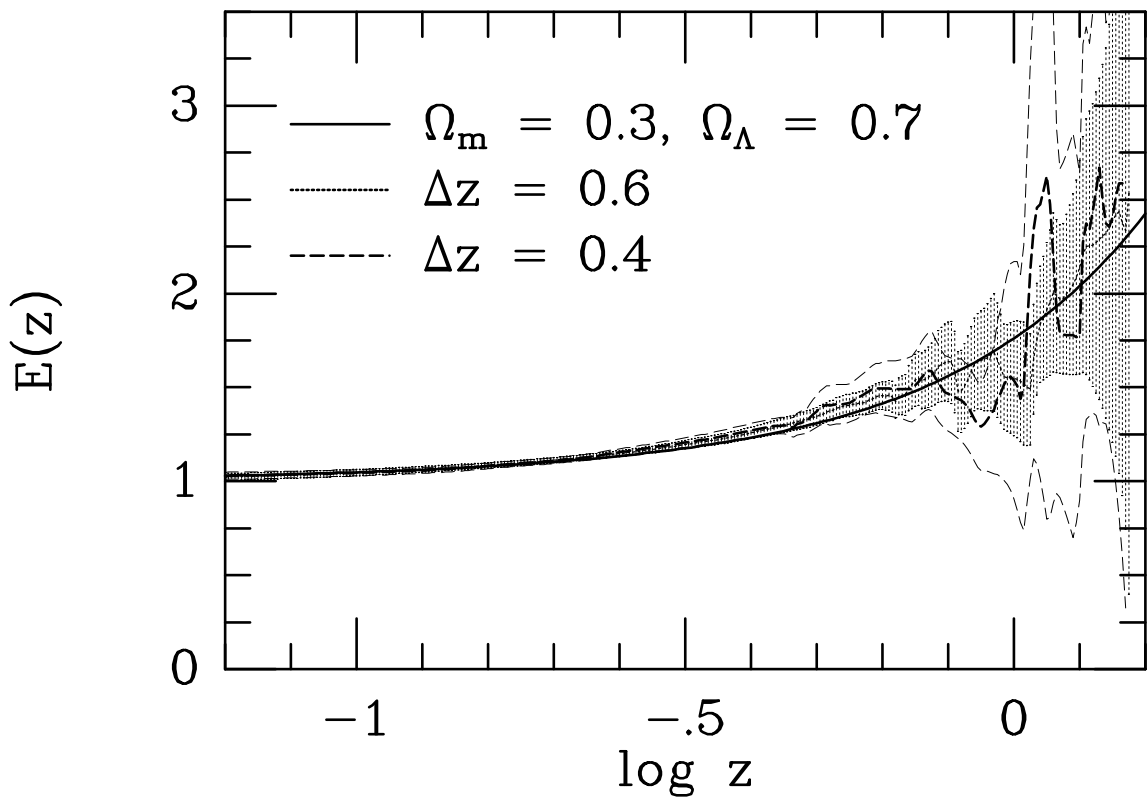


Fig. 6.— A first look at $E(z)$ for the full data set. Fits with $\Delta z = 0.6$ are shown with the thick dotted line, with the dotted hash indicating the $\pm 1\sigma$ range, and fits with $\Delta z = 0.4$ are shown with the thick dashed line, with the thin dashed lines indicating the $\pm 1\sigma$ range. The thick solid line shows the trend for the $\Omega_m = 0.3$, and $\Omega_\Lambda = 0.7$ Friedmann-Lemaître cosmology.

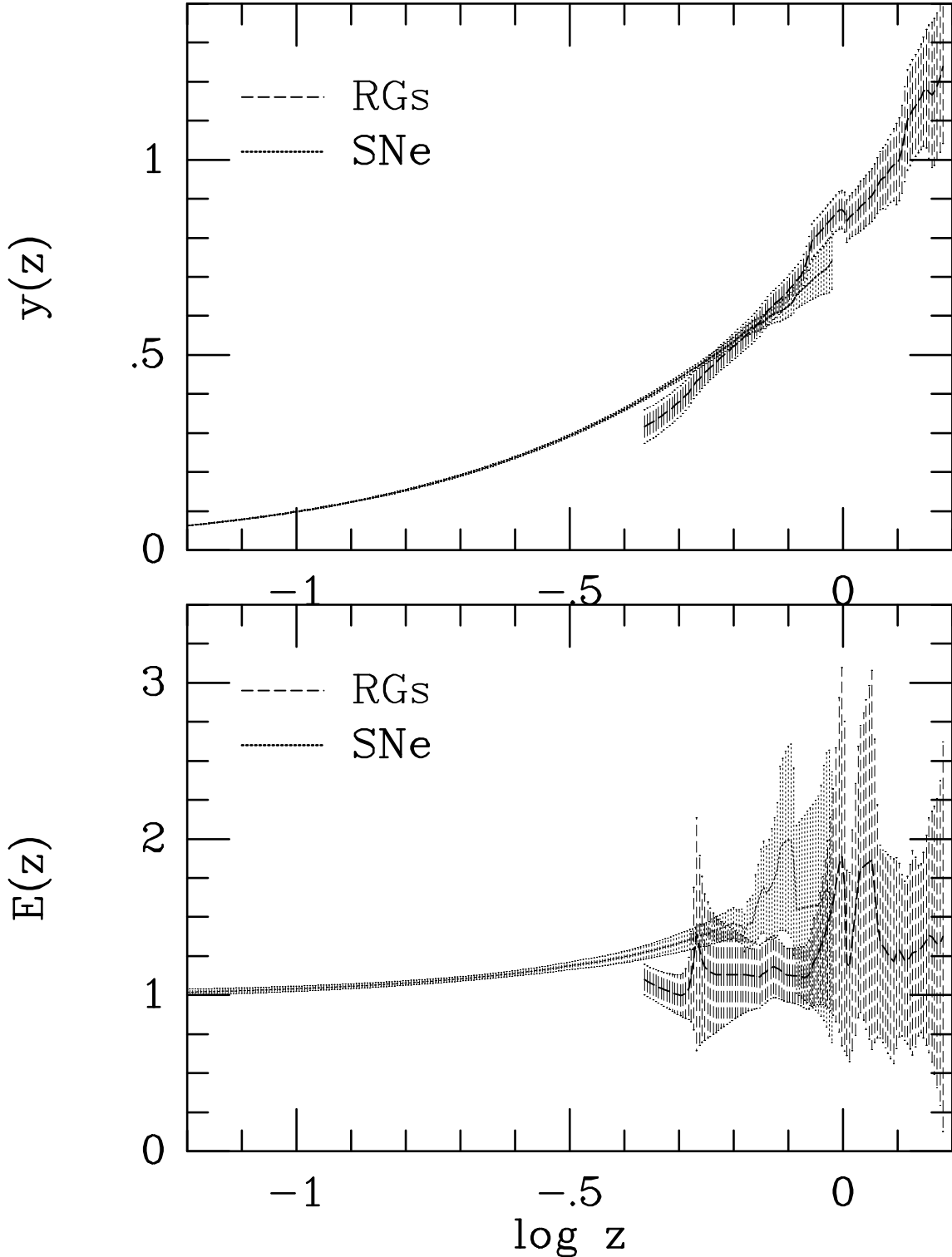


Fig. 7.— A comparison of the fits for SN and RG data sets separately; values of y_s for RGs were used for this fit. The SN data are shown as the dotted line and the dotted hatched area (the best fit values and the $\pm 1\sigma$ range); the corresponding fits for RGs are shown with the dashed line and hatched area.

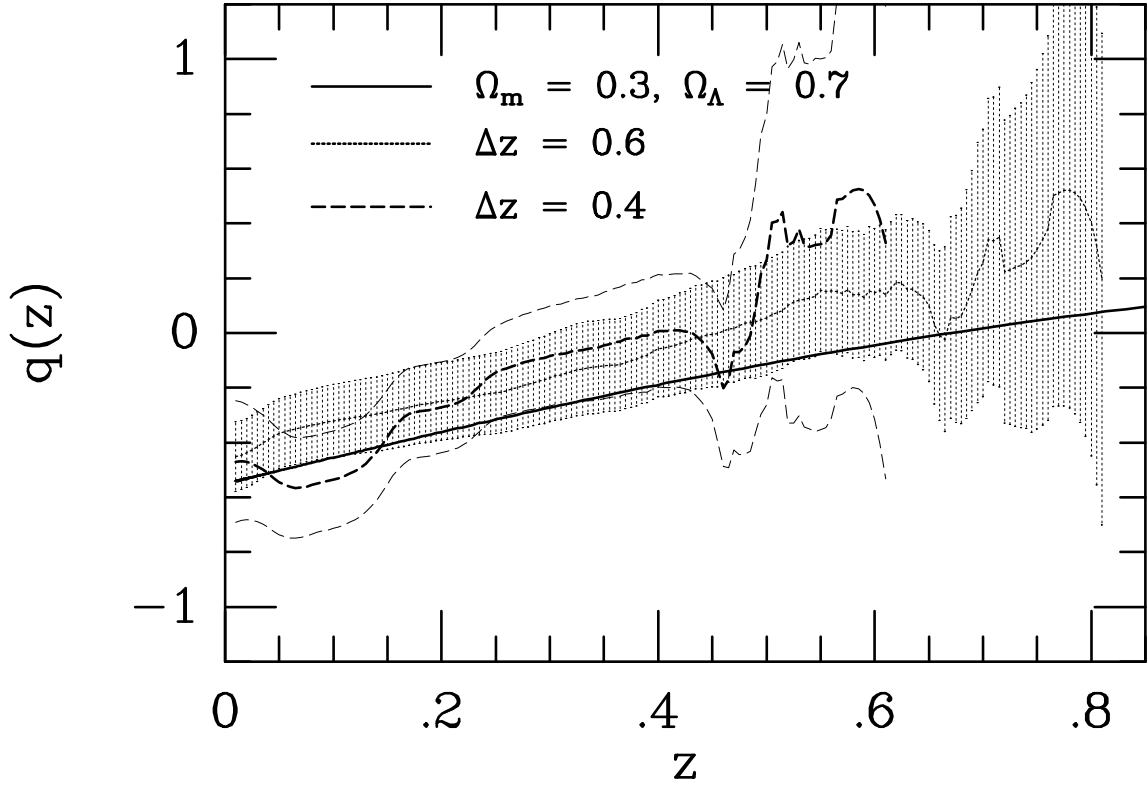


Fig. 8.— A first look at $q(z)$, obtained for the full data set. Fits with $\Delta z = 0.6$ are shown with the thick dotted line, with the dotted hash indicating the $\pm 1\sigma$ range, and fits with $\Delta z = 0.4$ are shown with the thick dashed line, with the thin dashed lines indicating the $\pm 1\sigma$ range. The thick solid line shows the trend for the $\Omega_m = 0.3$, and $\Omega_\Lambda = 0.7$ Friedmann-Lemaitre cosmology. The fits become too noisy to be useful past about $z \sim 0.8$ in this data set.

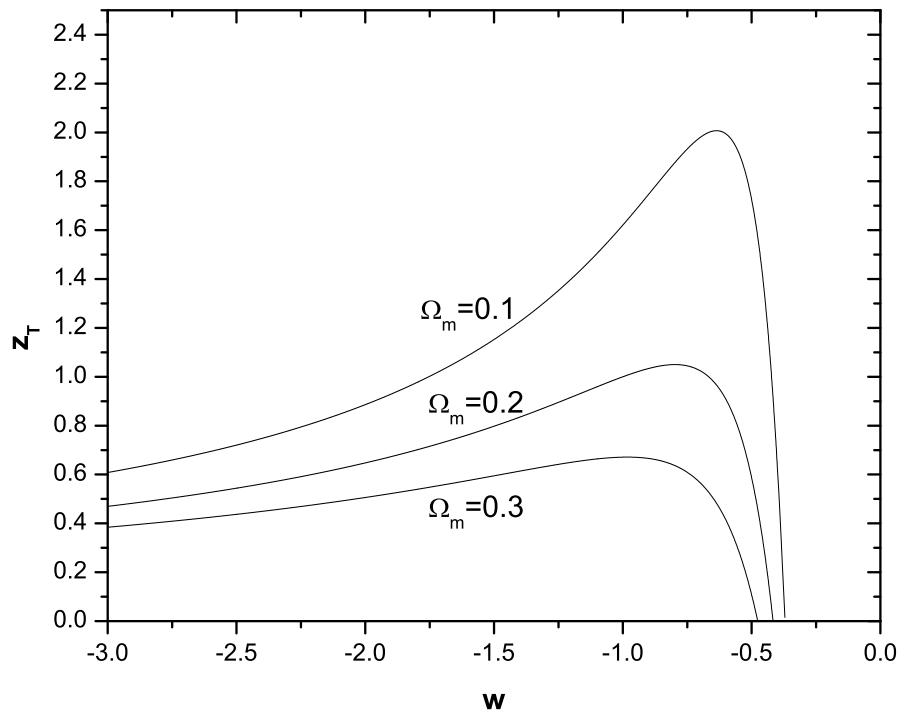


Fig. 9.— The transition redshift, z_T , at which the universe transitions from a state of deceleration to a state of acceleration, is plotted as a function of the equation of state of the dark energy assuming that the equation of state of the dark energy is time-indepedent. If equation (5) indicates a lower limit of the transition redshift, then bounds may be placed on the amount and redshift evolution of the dark energy.